ACS OMEGA

Open Access

http://pubs.acs.org/journal/acsodf

Article

Plasmonic Color Switching by a Combination Device with Nematic Liquid Crystals and a Silver Nanocube Monolayer

Ayana Mizuno, Yosei Shibata, Hideo Fujikake, and Atsushi Ono*

Cite This: *ACS Omega* 2023, 8, 41579−41585

Read Online

ACCESS | Metrics & More | Article Recommendations | Supporting Information

ABSTRACT: We experimentally demonstrated electrical plasmonic color modulation by combining a nematic-phase liquid crystal (LC) layer and a silver nanocube (AgNC) monolayer. The color modulation LC/AgNC device was fabricated by filling LCs with negative dielectric anisotropy onto a densely assembled AgNC monolayer. The transmitted light color through the LC/AgNC device was modulated between green and magenta by applying voltages of 0−15 V. The peaks and dips in the transmission spectrum of the LC/AgNC device at wavelengths of 500−600 nm were switched with voltage. The switching effect of light transmission in the green region was achieved by overlapping the plasmon resonance of the AgNC monolayer and multiple transmittance peaks caused by the birefringence of the LC layer. In addition, the color inversion appeared at cross-Nicole and parallel-Nicole because the LC layer functioned like a half-wave plate due to birefringence. The electrical modulation of the plasmonic color with LCs has a high implementation capability in microdevices and is anticipated to be applied in display devices or color filters.

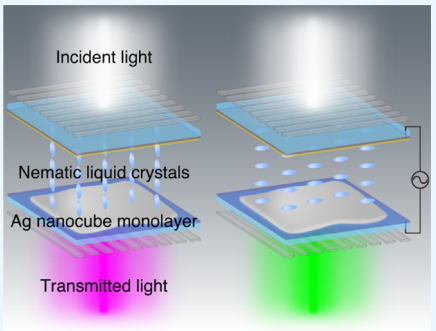

INTRODUCTION

Dynamic control of plasmon resonance has attracted attention due to its unique optical properties such as color modulation,[1−7] light intensity modulation,[8,9] and spectroscopy.[10,11] It has been actively investigated for many applications, including color filters,[2,3,5] colorimetric sensors,[7,12−14] and optical sensors.[8,15] In particular, electrical plasmon resonance control has been a popular research topic because of its many advantages such as high repeatability, fast response time, and compatibility for implementation in microdevices. Electrically dynamic tuning of plasmon resonance has been proposed and developed using liquid crystals (LCs),[2,5,7,8,16−21] conductive polymers,[22,23] organic electrolyte solvents,[3,24,25] and microelectromechanical system (MEMS) technology.[26,27] It is expected to lead to practical applications in ultracompact spectrometers and tunable color filters for multi- or hyperspectral image sensors with high light utilization efficiency.

The nanoscale refractive index anisotropy of LC molecules provides high electric polarizability by a strong interaction with plasmonic nanostructures. The alignment and birefringence of the LC molecules were electrically switched on the millisecond time scale, resulting in fast phase modulation. Therefore, LCs are applied in displays,[28−31] spatial light modulators (SLM),[32−34] and beam steering reflectors.[35−37]

The plasmon resonance dynamic tuning based on LCs has been mainly reported on the control of refractive index,[2,16−19] incident polarization,[5,7,8] and alignment of metal nanoparticles.[20,21] The anisotropic refractive index between the normal (n_o) and extraordinary (n_e) states of the LCs is reversibly tuned by the electric field alignment of LC molecules. The variations in the average refractive index surrounding the plasmonic nanostructures under an LC layer dynamically tune the plasmon resonance and the plasmonic color through applied voltages. In 2015, Franklin et al. used highly birefringent LCs ($\Delta n \sim 0.4$) coated on a shallow Al nanowell array to achieve a fairly broad plasmon tuning range of 95 nm.[2] The LCs on the shallow nanowells were completely reoriented, and the refractive index was controlled. The continuous color tuning from orange to green at 0 to 13.6 V/μm was demonstrated with a polarization-independent LC-plasmonic system.

The birefringence of the LCs with the applied voltages rotates the polarization states of the incident light. The plasmon resonance corresponding to the metallic nanostructures with asymmetric periodicity in the *x*- and *y*-directions is dynamically selected by switching the incident polarization with the LC, and the associated color is modulated. The linearly *y*-polarized incident light is rotated to *x*-polarized light by the twisted nematic (TN) LC in the off state. In 2017, Lee et al. fabricated an anisotropic nanohole array of rectangular lattices and incorporated a TN-LC layer on top of it. The molecular orientation of the LCs was electrically switched to achieve polarization-dependent extraordinary optical transmission (EOT).[5] The transmitted color significantly changed

Received: August 3, 2023
Revised: October 5, 2023
Accepted: October 17, 2023
Published: October 28, 2023

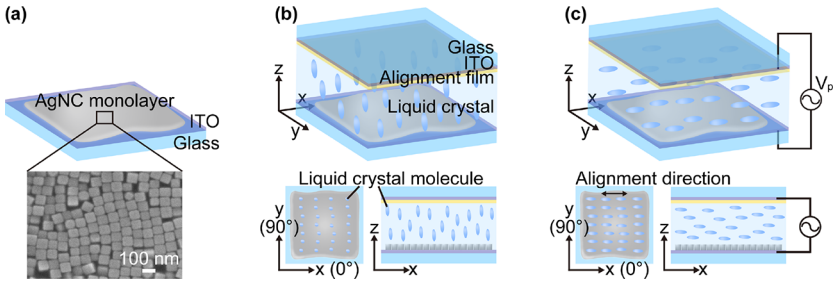

Figure 1. Schematic images of the proposed plasmonic color-switching device. (a) AgNC monolayer fabricated on a glass substrate with ITO thin film. (b) Vertical electric field-driven LC/AgNC device without voltages. LC molecules are oriented perpendicular to the substrate. (c) With voltages. The short axes of the LC molecules are oriented in parallel to the electric field.

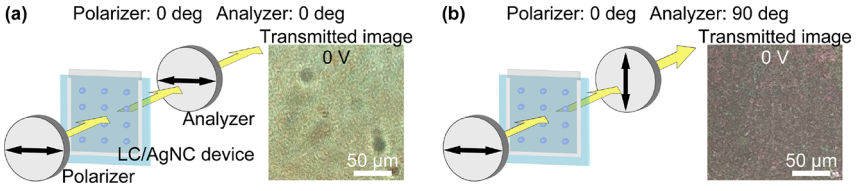

Figure 2. Transmitted light microscopic images of the LC/AgNC device: (a) parallel-Nicole (polarizer: 0°, analyzer: 0°); (b) cross-Nicole (polarizer: 0°, analyzer: 90°).

from blue-to-green or green-to-red on a millisecond order (~7 ms) with an applied voltage of 0 to 5 V.

Furthermore, anisotropic metal nanoparticles, such as nanorods and nanoplates, embedded in an LC host were aligned in the orientation direction by applied voltages. The two plasmon modes of anisotropic metal nanoparticles were selectively excited by switching the applied voltage with the linear polarization of incident light. In 2014, Liu et al. integrated Au nanorods aligned parallel to the average local LC molecular alignments.[20] The longitudinal plasmon mode of short nanorods was excited by polarized light in the LC molecular alignment direction at 0 V, and the LC composite appeared green. The LC molecules and nanorods were aligned vertically by applying the voltage. The transverse plasmon mode was excited over 4 V, causing the red-color appearance. These techniques achieved dynamic resonance wavelength shifts of the plasmonic nanostructures in the LC layer due to the switching of the LC molecule alignment in response to voltage.

We focused on crystalline silver nanocubes (AgNCs) as plasmonic materials. The cube shape provides higher plasmon resonance due to the smaller dispersion of electron vibrations compared to the sphere shape, leading to a narrow-band spectrum and a clear resonance shift. AgNCs greatly enhance the electric field at their sharp corners due to dipole or quadrupole local surface plasmon resonance; this enhancement has been applied to surface-enhanced Raman scattering (SERS),[38,39] photocurrent enhancement for solar cells,[40,41] and spontaneous emission sources.[42,43] In addition, Ag is suitable for surface plasmon excitation at visible wavelengths since it has the lowest absorption losses among all metals. Our previous research has demonstrated mechanical plasmonic color modulation using a self-assembled AgNC monolayer in a stretchable polydimethylsiloxane (PDMS) substrate.[44] The rising wavelength of the long-pass transmission band blue-shifted when the plasmon mode of the AgNC monolayer was controlled through PDMS substrate stretching. Accordingly, the transmitted light color was dynamically tuned from magenta to yellow. High plasmon resonance and clear transmitted light color modulation were obtained with the AgNC monolayer.

Here, we proposed an LC device combined with a crystalline AgNC monolayer for electrically switching the transmission color through applied voltages. The transmission peak wavelengths were shifted due to the birefringence of the LCs by applying bias. The convolution of the birefringence-induced wavelength shift and the transmission spectrum associated with AgNCs' plasmon resonance resulted in a spectral color shift. The high plasmon resonance of the AgNCs was utilized to achieve clear color modulation. A crystalline AgNC has flat facets, and a close-packed assembled layer of AgNCs provides a plasmonic substrate with a smooth surface because their facets face up. Therefore, the AgNC monolayer is suitable for LC devices in terms of suppression of alignment disorder.

RESULTS AND DISCUSSION

Fabrication of the LC/AgNC Hybrid Device. Figure 1 shows a schematic diagram of the proposed plasmonic color modulation device, which consists of a close-packed Ag nanocube (AgNC) monolayer combined with an LC layer. The AgNC monolayer was fabricated by the Langmuir–Blodgett (LB) method on an indium–tin oxide (ITO)-coated glass substrate that was utilized as the bottom electrode (Figure 1a). The synthesis and assembly processes of the AgNC monolayer are provided in the Experimental Section. The AgNC monolayer was fabricated with an edge length of approximately 100 nm and a cube density of 133.7 cubes/μm^2. An ITO-coated glass substrate with an aligned polyimide film formed by rubbing in the x-axis direction was used as the counter substrate. A spacer layer was formed between both substrates with a thickness of 12 μm using silica spacers, and the LCs were vacuum-injected into the layer. In our proposed color modulation LC/AgNC device, the VA (vertical alignment) LCs were used as the initial alignment state to suppress the light scattering behavior (haze). The LCs were horizontally oriented by varying the applied voltages between the two substrates, leading to plasmonic color modulation. Since the LCs were a negative type, the vertically aligned initial state

https://doi.org/10.1021/acsomega.3c05707
ACS Omega 2023, 8, 41579−41585

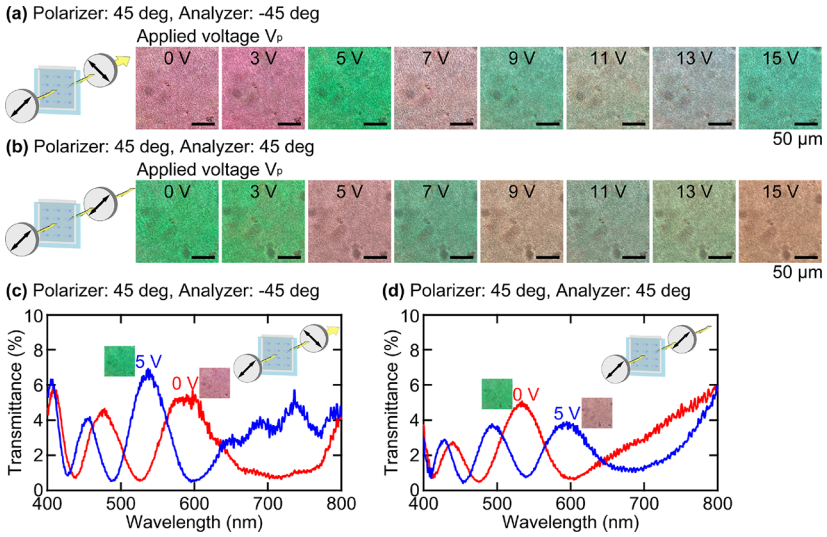

Figure 3. Plasmonic color modulation with applied voltage from 0 to 15 V at (a) cross-Nicole and (b) parallel-Nicole. The color of transmitted light through the LC/AgNC device was modulated between magenta and green as the voltage was applied. Transmission spectra of the LC/AgNC device at applied voltages of 0 and 5 V under (c) cross-Nicole and (d) parallel-Nicole. In the green-wavelength range of approximately 530 nm, the transmission peaks and dips observed at applied voltages of 0 and 5 V were inverted between the cross-Nicole and parallel-Nicole.

(Figure 1b) oriented in-plane (Figure 1c) in an electrically saturated state. The refractive indices of LCs were 1.509 (n_e) and 1.306 (n_o) at a wavelength of 589 nm.

Figure 2 shows the transmitted light microscopic images of the LC/AgNC device without a voltage applied. The transmitted light from the device was bright at parallel-Nicole (polarizer: 0°, analyzer: 0°) and dark at crossed-Nicole (polarizer: 0°, analyzer: 90°). Birefringence did not occur without an applied voltage, indicating that the LC/AgNC device showed little disorder in the LC alignment.

Electrical Plasmonic Color Modulation. Figure 3a,b shows the transmitted light microscopic images of the color modulation LC/AgNC device with an applied voltage from 0 to 15 V (Vp). The incident polarization was set to 45°. Light transmission was observed in the cross-Nicole as well as in parallel due to the birefringence caused by driving the LCs with the applied voltage. The color of light transmitted through the LC/AgNC device in the cross-Nicole was magenta at an applied voltage of 0 V and green at an applied voltage of 5 V. However, the color in the parallel-Nicole was green at 0 V and magenta at 5 V. The transmitted light color reversed several times between magenta and green as the voltage increased. In addition, the colors of transmitted light were inverted between the cross-Nicole and parallel-Nicole at each applied voltage. The imperfect initial VA caused the light transmission at 0 V in the cross-Nicole because some LC molecules were tilted in the pretilt direction. Ideally, the initial orientation of the molecules should be vertical, but in this particular case, the LCs become randomly oriented in the lateral plane under biased conditions. To achieve uniform LC molecular orientation under bias for the birefringence, a pretilt process is necessary. Therefore, the birefringence effect was observed even at 0 V.

Figure 3c,d shows the transmission spectra of the LC/AgNC device at 0 and 5 V, which exhibited clear color inversion. Multiple transmission peaks originating from the birefringence shifted with a voltage in the visible region. The transmission peaks between 0 and 5 V were nearly identical in the blue-wavelength region, whereas they were inverted in the green-wavelength region. The opposite behavior was shown between the cross-Nicole and the parallel-Nicole. Focusing on 500−600 nm, the transmitted light colors green and magenta corresponded to the peak and dip of the spectrum.

Analysis of Transmission Spectrum. We investigated in more detail the transmission spectra of the LC/AgNC device with applied voltages to elucidate the color inversion. Figure 4a,b shows the transmission spectra of the LC/AgNC device at applied voltages from 0 to 15 V. The amplitude of the transmission was not constant in the spectra. The spectral envelope showed a peak at a wavelength of 535 nm in both polarization states. The shape of the spectral envelope was in good agreement with the transmission spectrum of the AgNC monolayer before LC filling, as shown in Figure S1. Therefore, the peak of the envelope was attributed to the plasmon

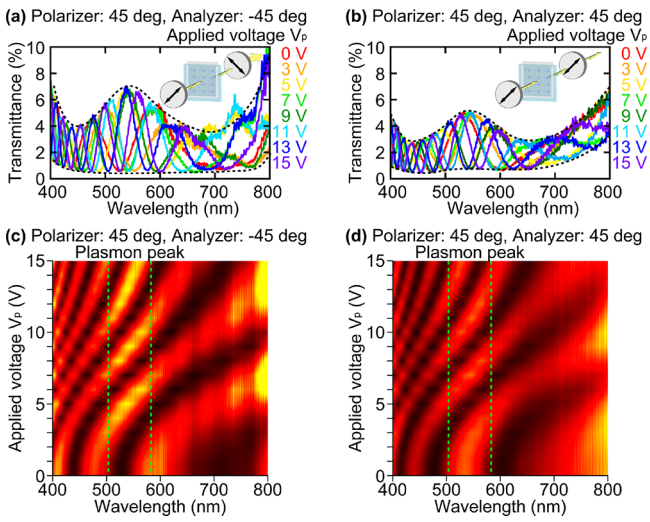

Figure 4. Line profile and two-dimensional map of the LC/AgNC device's transmission spectra for applied voltage from 0 to 15 V at (a, c) cross-Nicole and (b, d) parallel-Nicole. A transmission peak was observed at wavelengths of 500−600 nm due to the plasmon resonance of the AgNC monolayer.

https://doi.org/10.1021/acsomega.3c05707
ACS Omega 2023, 8, 41579−41585

resonance of the AgNC monolayer based on the hybridization plasmon mode of the local and collective oscillation modes.

Figure 4c,d shows the two-dimensional map of the transmission spectra for different applied voltages from 0 to 15 V. The transmission peak shifted to longer wavelengths with applied voltage, and the number of peaks increased. This characteristic was caused by the increase in the refractive index difference associated with the percentage increase in the abnormal refractive index (n_e) owing to birefringence and resulted in an increased optical path length. The number of peaks derived from birefringence was reasonable at saturated voltages when the LC layer had a thickness of 12 μm with a refractive index difference of ∼0.2. The transmission peaks were inverted at each applied voltage in the cross-Nicole and parallel-Nicole. The LC layer functioned like a half-wave plate due to the birefringence of the LCs. Moreover, in the wavelength range of 500 to 600 nm, the overlap of the spectra with birefringence and the surface plasmon resonance of the AgNC monolayer caused a higher transmittance, producing a green color as the transmitted light. In contrast, when the spectral dip coincided with the plasmon resonance wavelength, the transmitted light color was magenta because the transmission peak of AgNCs was canceled out by the birefringence. In summary, the disordered transmission spectral shapes of the LC/AgNC device were caused by the convolution of the birefringence and the plasmon resonance of the AgNC monolayer. Accordingly, the plasmonic color modulation between green and magenta was obtained.

Simulation of the LC Layer. For comparison, we simulated the transmission spectra of the birefringence in the LC layer using Optics Master (LCD Master 1D, SHINTECH Co., Ltd.) to corroborate the contribution of the AgNC monolayer plasmon to the color modulation. Figure 5a,b shows the simulated transmission spectra of the LC layer with a thickness of 12 μm at applied voltages from 0 to 15 V. The AgNC monolayer was not included in the simulation model. The transmission peaks red-shifted with the applied voltage, and the number of peaks increased to the same extent as in the experimental spectra. The amplitude of the transmission spectra was constant with the applied voltage. The peak in the envelope was not observed as in the LC/AgNC device spectra shown in Figure 4a,b. Figure 4 shows the transmission spectral data for the LC/AgNC-combined device, whereas Figure S1 and Figure 5 correspond to the individually separated data for AgNC only and LC device only. According to these results, the plasmon resonance in the AgNC monolayer contributed to electrical light transmission switching in the green region.

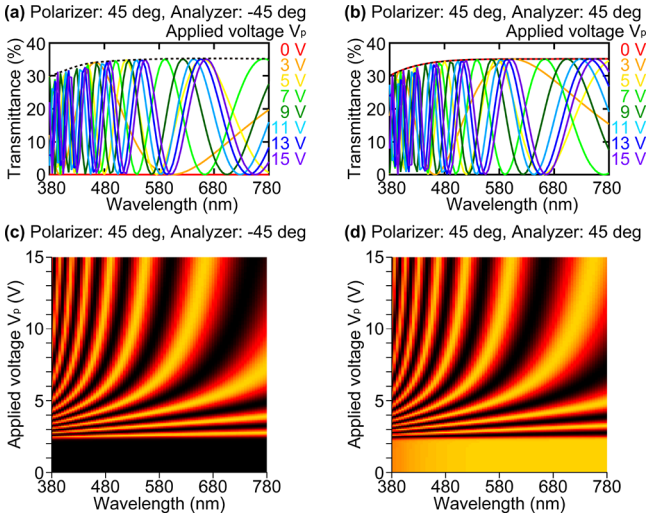

Figure 5. Simulation of the wavelength-transmittance characteristics of a vertically oriented LC cell with a thickness of 12 μm at (a) and (c) cross-Nicole and (b and (d) parallel-Nicole. The envelope of the transmission spectra was constant, and high transmittance was not observed in a specific wavelength region.

Figure 5c,d shows the two-dimensional map of the simulated transmission spectra for different applied voltages from 0 to 15 V. Higher transmittance at specific wavelengths was not observed, as shown in the LC/AgNC device 2D maps in Figure 4c,d. Focusing on applied voltages at 0 and 3 V, no light and white light transmissions were appeared at the cross-Nicole and the parallel-Nicole, respectively. The LC alignment in the simulation was ideal, whereas the LC/AgNC device was disordered perpendicular to the initial LC alignment. This disorganization was caused by the attraction and trapping of LC molecules on the surface of the AgNCs due to the surface anchoring force. In addition, small assembled defects in the monolayer were the starting point for the discontinuous LC alignment defects, leading to LC disclination. These factors led to the disruption of the VA of the LCs near the surface of the AgNC monolayer. Therefore, the random alignment caused birefringence, which resulted in light transmission at the crossed-Nicole without an applied voltage. As a result, the clear color switching by voltage ON and OFF was obtained due to alignment disorder.

CONCLUSIONS

We successfully demonstrated electrical plasmonic color switching between green and magenta by applying voltages to the LC layer and the AgNC monolayer hybrid device. Nanocubes with an edge length of approximately 100 nm were synthesized through a polyol process, and their close-packed monolayer was fabricated by using the LB method on an ITO-glass substrate. The color modulation device was fabricated by filling negative LCs with a thickness of 12 μm onto a densely assembled AgNC monolayer. The transmitted light color through the LC/AgNC device was modulated between magenta and green by applying voltages of 0−15 V under cross-Nicole and parallel-Nicole. The convolution of the birefringence of the LC layer and the plasmon resonance of the AgNC monolayer provided a switching effect of the light transmittance in the green region. In addition, the color inversion appeared at the cross-Nicole and parallel-Nicole positions due to the half-wave phase modulation caused by the birefringence of the LC layer. Electrically plasmonic color modulation is advantageous in terms of response speed and implementation capability and is anticipated to facilitate the development of tunable optical filters. In our research, the initial VA disorder of the LC layer caused birefringence, resulting in light transmission at the cross-Nicole at a voltage of 0 V. Clear plasmonic color switching with voltage ON and OFF is important for practical applications, such as display devices and anticounterfeit tags.

EXPERIMENTAL SECTION

Materials. Polyvinylpyrrolidone (PVP) (M_w = 55 000 g/mol), ethylene glycol (99.8%), and hydrochloric acid (37%,

https://doi.org/10.1021/acsomega.3c05707
ACS Omega 2023, 8, 41579−41585

ACS reagent) were purchased from Sigma−Aldrich and used without further purification. Silver nitrate (≥99.8%) was purchased from FUJIFILM Wako Pure Chemical Corporation.

Fabrication of the Ag Nanocube Monolayer. The crystalline Ag nanocubes were synthesized by a polyol process with HCl based on the recipe in Xia et al.'s paper.[45,46] In the polyol process used in this study, ethylene glycol (EG), silver nitrate, and PVP were used as the solvent and reducing agent, the silver ion source, and the polymer capping agent, respectively. In addition, hydrochloric acid was used as an oxidative etching agent for the silver seeds and facet control of Ag nanocubes.[47,48] In a typical synthesis, 2 mL of EG was placed in a 100 mL glass vial and preheated to 145 °C without a cap while being stirred in an oil bath. After 1 h, 0.333 mL of 2.7 mM HCl was added to the EG and the vial was capped. Ten minutes after the addition of HCl, 1 mL of 90 mM $AgNO_3$ in EG solution and 1 mL of 135 mM PVP in EG solution were simultaneously injected into the EG via two-channel syringes at 0.75 mL/min. Then, the vial was tightly capped. After 24 h of stirring, the vial was removed from the oil bath and cooled with water. The synthesized Ag nanocube solution was separated by centrifugation at 3000 rpm for 20 min. The excess EG and PVP were removed, and the Ag nanocubes were dissolved in a mixture of water and ethanol. In addition, the Ag nanocube solution was filtered by syringes with hole diameters of 0.45 and 0.22 μm to exclude byproducts, such as Ag nanowires. The purified Ag nanocubes were dispersed in 200 μL of ethanol and 500 μL of toluene for the LB method. A total of 700 μL of the Ag nanocube colloid in toluene was added dropwise on the water surface of LB equipment. After the sample was allowed to sit for 1 h to volatilize toluene, the barrier arms moved at 27.07 mm/min from both sides of the LB equipment. The barriers were moved until the Ag nanocube layer on the water surface exhibited a metallic luster, and the ITO-coated glass substrate was dipped into the Ag nanocube layer from above to transfer the Ag nanocube onto the substrate.

Fabrication of the LC/AgNC Monolayer Device. The glass substrate with an ITO transparent electrode (150 nm) was cleaned with ultrasonication and alkaline conditions. The polyimide (SE-4811, Nissan Chemical Corp.) was coated onto the cleaned substrate by spin-coating at 3000 rpm for 30 s and was baked in an oven at 130 °C for 1 h to remove the polyimide solvent. The thickness of the polyimide film was 50 nm. The polyimide thin film was rubbed to align the LC molecules. The rubbing roller was rotated at 1000 rpm with a depth of 0.1 mm, and the substrate was moved at 0.3 mm/s. The direction of these grooves was correlated with the alignment direction of the LC molecules. A UV-curable resin containing silica beads (microporous) was dispensed around the substrate to form a spacer layer. The estimated gap between the upper and lower substrates was 12 μm. The AgNC monolayer fabricated on the ITO-coated glass substrate was placed on top of the UV-curable resin as a counter substrate. The UV irradiation conditions included a wavelength of 365 nm and an intensity of 10 mJ intensity. The surrounding region with the spacer was filled with LCs by a vacuum injection method. The substrate was fixed in a vacuum at ∼4 × 10 Pa, and the *z*-axis movable table was raised to immerse the inlet into the LCs. LCs were injected into the spacer layer by restoring the vacuum to atmospheric pressure.

Optical Characterization. The transmission spectra of the LC/AgNC device were measured using a halogen lamp (FHL-101, Asahi Spectra Co., Ltd.) and spectrometer (MAYA2000P-RO, Ocean Insights Ltd.). Microscopic transmission images were captured with a microscope (Olympus Corp.) and a charge-coupled-device (CCD) camera (LEICA DFC7000 T, Leica). White LED light was uniformly irradiated over the entire observation area.

■ ASSOCIATED CONTENT

Supporting Information

The Supporting Information is available free of charge at https://pubs.acs.org/doi/10.1021/acsomega.3c05707.

Polarized incident transmission spectra of the AgNC monolayer without LCs (PDF)

■ AUTHOR INFORMATION

Corresponding Author

Atsushi Ono − *Graduate School of Science and Technology, Shizuoka University, Hamamatsu 432-8561, Japan; Research Institute of Electronics, Shizuoka University, Hamamatsu 432-8011, Japan;* orcid.org/0000-0002-7816-3614; Email: ono.atsushi@shizuoka.ac.jp

Authors

Ayana Mizuno − *Graduate School of Science and Technology, Shizuoka University, Hamamatsu 432-8561, Japan*

Yosei Shibata − *Department of Electronic Engineering, Graduate School of Engineering, Tohoku University, Sendai 980-8579, Japan*

Hideo Fujikake − *Department of Electronic Engineering, Graduate School of Engineering, Tohoku University, Sendai 980-8579, Japan*

Complete contact information is available at: https://pubs.acs.org/10.1021/acsomega.3c05707

Notes

The authors declare no competing financial interest.

■ ACKNOWLEDGMENTS

We acknowledge the stimulated discussion in the meeting of the Cooperative Research Project of the Research Institute of Electrical Communication, Tohoku University.

■ REFERENCES

(1) Ellenbogen, T.; Seo, K.; Crozier, K. B. Chromatic plasmonic Polarizers for Active Visible Color Filtering and Polarimetry. *Nano Lett.* **2012**, *12* (2), 1026−1031.

(2) Franklin, D.; Chen, Y.; Guardado, A. V.; Modak, S.; Boroumand, J.; Xu, D.; Wu, S. T.; Chanda, D. Polarization-independent actively tunable colour generation on imprinted plasmonic surfaces. *Nat. Commun.* **2015**, *6*, 7337.

(3) Wang, G.; Chen, X.; Liu, S.; Wong, C.; Chu, S. Mechanical Chameleon through Dynamic Real-Time plasmonic Tuning. *ACS Nano* **2016**, *10* (2), 1788−1794.

(4) Song, S.; Ma, X.; Pu, M.; Li, X.; Liu, K.; Gao, P.; Zhao, Z.; Wang, Y.; Wang, C.; Luo, X. Actively Tunable Structural Color Rendering with Tensile Substrate. *Adv. Optical Mater.* **2017**, *5* (9), 1600829.

(5) Lee, Y.; Park, M. K.; Kim, S.; Shin, J. H.; Moon, C.; Hwang, J. Y.; Choi, J. C.; Park, H.; Kim, H. R.; Jang, J. E. Electrical Broad Tuning of plasmonic Color Filter Employing an Asymmetric-Lattice Nanohole Array of Metasurface Controlled by Polarization Rotator. *ACS Photonics* **2017**, *4* (8), 1954−1966.

(6) Tseng, M. L.; Yang, J.; Semmlinger, M.; Zhang, C.; Nordlander, P.; Halas, N. J. Two-Dimensional Active Tuning of an Aluminum

plasmonic Array for Full-Spectrum Response. *Nano Lett.* **2017**, *17* (10), 6034−6039.
(7) Sharma, M.; Hendler, N.; Ellenbogen, T. Electrically Switchable Color Tags Based on Active Liquid-Crystal plasmonic Metasurface Platform. *Adv. Optical Mater.* **2020**, *8* (7), 1901182.
(8) Buchnev, O.; Ou, J. Y.; Kaczmarek, M.; Zheludev, N. I.; Fedotov, V. A. Electro-optical control in a plasmonic metamaterial hybridised with a liquid-crystal cell. *Opt. Express* **2013**, *12* (2), 1633−1638.
(9) Sterl, F.; Strohfeldt, N.; Walter, R.; Griessen, R.; Tittl, A.; Giessen, H. Magnesium as Novel Material for Active Plasmonics in the Visible Wavelength Range. *Nano Lett.* **2015**, *15* (12), 7949−7955.
(10) Xu, B. B.; Ma, Z. C.; Wang, H.; Liu, X. Q.; Zhang, Y. L.; Zhang, X. L.; Zhang, R.; Jiang, H. B.; Sun, H. B. A SERS-active microfluidic device with tunable surface plasmon resonances. *Electrophoresis* **2011**, *32* (23), 3378−3384.
(11) Byers, C. P.; Hoener, B. S.; Chang, W. S.; Yorulmaz, M.; Link, S.; Landes, C. F. Single-Particle Spectroscopy Reveals Heterogeneity in Electrochemical Tuning of the Localized Surface Plasmon. *J. Phys. Chem. B* **2014**, *118* (49), 14047−14055.
(12) Wang, Z.; Lee, J. H.; Lu, Y. Label-Free Colorimetric Detection of Lead Ions with a Nanomolar Detection Limit and Tunable Dynamic Range by using Gold Nanoparticles and DNAzyme. *Adv. Mater.* **2008**, *20* (17), 3263−3267.
(13) King, N. S.; Liu, L.; Yang, X.; Cerjan, B.; Everitt, H. O.; Nordlander, P.; Halas, N. J. Fano Resonant Aluminum Nanoclusters for plasmonic Colorimetric Sensing. *ACS Nano* **2015**, *9* (11), 10628−10636.
(14) Liu, D.; Fang, L.; Zhou, F.; Li, H.; Zhang, T.; Li, C.; Cai, W.; Deng, Z.; Li, L.; Li, Y. Ultrasensitive and Stable Au Dimer-Based Colorimetric Sensors Using the Dynamically Tunable Gap-Dependent plasmonic Coupling Optical Properties. *Adv. Funct. Mater.* **2018**, *28* (18), 1707392.
(15) Jorgenson, R. C.; Yee, S. S. Control of the dynamic range and sensitivity of a surface plasmon resonance based fiber optic sensor. *Sensors and Acmetom A* **1994**, *43* (1−3), 44−48.
(16) Kossyrev, P. A.; Yin, A.; Cloutier, S. G.; Cardimona, D. A.; Huang, D.; Alsing, P. M.; Xu, J. M. Electric Field Tuning of plasmonic Response of Nanodot Array in Liquid Crystal Matrix. *Nano Lett.* **2010**, *5* (10), 1978−1981.
(17) Liu, Y. J.; Si, G. Y.; Leong, E. S. P.; Xiang, N.; Danner, A. J.; Teng, J. H. Light-Driven plasmonic Color Filters by Overlaying Photoresponsive Liquid Crystals on Gold Annular Aperture Arrays. *Adv. Mater.* **2012**, *24* (23), OP131−OP135.
(18) Zou, C.; Komar, A.; Fasold, S.; Bohn, J.; Muravsky, A. A.; Murauski, A. A.; Pertsch, T.; Neshev, D. N.; Staude, I. Electrically Tunable Transparent Displays for Visible Light Based on Dielectric Metasurfaces. *ACS Photonics* **2019**, *6* (6), 1533−1540.
(19) Ghosh, S.; Smalyukh, I. Electrical Switching of Nematic plasmonic Nanocolloids for Infrared Solar Gain Control. *Adv. Opt. Mater.* **2022**, *10*, 2201513.
(20) Liu, Q.; Yuan, Y.; Smalyukh, I. I. Electrically and Optically Tunable plasmonic Guest−Host Liquid Crystals with Long-Range Ordered Nanoparticles. *Nano Lett.* **2014**, *14* (7), 4071−4077.
(21) Zhang, Y.; Liu, Q.; Mundoor, H.; Yuan, Y.; Smalyukh, I. I. Metal Nanoparticle Dispersion, Alignment, and Assembly in Nematic Liquid Crystals for Applications in Switchable plasmonic Color Filters and E-Polarizers. *ACS Nano* **2015**, *9* (3), 3097−3108.
(22) Xu, T.; Walter, E. C.; Agrawal, A.; Bohn, C.; Velmurugan, J.; Zhu, W.; Lezec, H. J.; Talin, A. A. High-contrast and fast electrochromic switching enabled by plasmonics. *Nat. Commun.* **2015**, *7*, 10479.
(23) Xiong, K.; Emilsson, G.; Maziz, A.; Yang, X.; Shao, L.; Jager, E. W. H.; Dahlin, A. B. plasmonic Metasurfaces with Conjugated Polymers for Flexible Electronic Paper in Color. *Adv. Mater.* **2016**, *28* (45), 9956−9960.
(24) Araki, S.; Nakamura, K.; Kobayashi, K.; Tsuboi, A.; Kobayashi, N. Electrochemical Optical-Modulation Device with Reversible Transformation Between Transparent, Mirror, and Black. *Adv. Mater.* **2012**, *24, 23*, OP122−OP126.
(25) Feng, Z.; Jiang, C.; He, Y.; Chu, S.; Chu, G.; Peng, R.; Li, D. Widely Adjustable and Quasi-Reversible Electrochromic Device Based on Core−Shell Au−Ag plasmonic Nanoparticles. *Adv. Optical Mater.* **2014**, *2* (12), 1174−1180.
(26) Yamaguchi, K.; Fujii, M.; Okamoto, T.; Haraguchi, M. Electrically driven plasmon chip: Active plasmon filter. *Appl. Phys. Express* **2014**, *7* (1), No. 012201.
(27) Honma, H.; Takahashi, K.; Ishida, M.; Sawada, K. Continuous control of surface-plasmon excitation wavelengths using nano-mechanically stretched subwavelength grating. *Appl. Phys. Express* **2016**, *9* (2), No. 027201.
(28) Heilmeier, G. H.; Zanoni, L. A.; Barton, L. A. Dynamic Scattering: A New Electrooptic Effect in Certain Classes of Nematic Liquid Crystals. *Proc. IEEE* **1968**, *56* (7), 1162−1171.
(29) Schadt, M.; Helfrich, W. VOLTAGE-DEPENDENT OPTICAL ACTIVITY OF A 1WISTED NEMATIC LIQUID CRYSTAL. *Appl. Phys. Lett.* **1971**, *18* (4), 127−128.
(30) Schadt, M.; Seiberle, H.; Schuster, A. Optical patterning of multi- domain liquid-crystal displays with wide viewing angles. *Nature* **1996**, *381*, 212−215.
(31) Chen, H. W.; Lee, J. H.; Lin, B. Y.; Chen, S.; Wu, S. T. Liquid crystal display and organic light-emitting diode display: present status and future perspectives. *Light: Science & Applications* **2018**, *7*, 17168.
(32) Weiner, A. M. Femtosecond pulse shaping using spatial light modulators. *Rev. Sci. Instrum.* **2000**, *71* (5), 1929−1960.
(33) Woltman, S. J.; Jay, G. D.; Crawford, G. P. Liquid-crystal materials find a new order in biomedical applications. *Nat. Mater.* **2007**, *6*, 929−938.
(34) Ostrovsky, A. S.; Rickenstorff-Parrao, C.; Arrizón, V. Generation of the "perfect" optical vortex using a liquid-crystal spatial light modulator. *Opt. Lett.* **2013**, *38* (4), 534−536.
(35) Hällstig, E.; Stigwall, J.; Lindgren, M.; Sjöqvist, L. Laser Beam Steering and Tracking using a Liquid Crystal Spatial Light Modulator. *Proc. SPIE* **2003**, *5087*, 13−23.
(36) Bildik, S.; Dieter, S.; Fritzsch, C.; Menzel, W.; Jakoby, R. Reconfigurable Folded Reflectarray Antenna Based Upon Liquid Crystal Technology. *IEEE Trans. Antennas Propag.* **2015**, *63*, 122−132.
(37) Li, X.; Sato, H.; Shibata, Y.; Ishinabe, T.; Fujikake, H.; Chen, Q. Development of Beam Steerable Reflectarray With Liquid Crystal for Both E-Plane and H-Plane. *IEEE Access* **2022**, *10*, 26177−26185.
(38) McLellan, J. M.; Li, Z. Y.; Siekkinen, A. R.; Xia, Y. The SERS Activity of a Supported Ag nanocube Strongly Depends on Its Orientation Relative to Laser Polarization. *Nano Lett.* **2007**, *7* (4), 1013−1017.
(39) Lee, H. K.; Lee, Y. H.; Zhang, Q.; Phang, I. Y.; Tan, J. M. R.; Cui, Y.; Ling, X. Y. Superhydrophobic Surface-Enhanced Raman Scattering Platform Fabricated by Assembly of Ag nanocubes for Trace Molecular Sensing. *ACS Appl. Mater. Interfaces* **2013**, *5* (21), 11409−11418.
(40) Baek, S. W.; Park, G.; Noh, J.; Cho, C.; Lee, C. H.; Seo, M. K.; Song, H.; Lee, J. Y. Au@Ag Core-Shell nanocubes for Efficient plasmonic Light Scattering Effect in Low Bandgap Organic Solar Cells. *ACS Nano* **2014**, *8* (4), 3302−3312.
(41) Kawawaki, T.; Wang, H.; Kubo, T.; Saito, K.; Nakazaki, J.; Segawa, H.; Tatsuma, T. Efficiency Enhancement of PbS Quantum Dot/ZnO Nanowire Bulk-Heterojunction Solar Cells by plasmonic Silver nanocubes. *ACS Nano* **2015**, *9* (4), 4165−4172.
(42) Akselrod, G. M.; Argyropoulos, C.; Hoang, T. B.; Ciracì, C.; Fang, C.; Huang, J.; Smith, D. R.; Mikkelsen, M. H. Probing the mechanisms of large Purcell enhancement in plasmonic nano-antennas. *Nat. Photonics* **2014**, *8*, 835−840.
(43) Fusella, M. A.; Saramak, R.; Bushati, R.; Menon, V. M.; Weaver, M. S.; Thompson, N. J.; Brown, J. J. plasmonic enhancement of stability and brightness in organic light-emitting devices. *Nature* **2020**, *585*, 379−382.
(44) Mizuno, A.; Ono, A. Dynamic Control of the Interparticle Distance in a Self-Assembled Ag nanocube Monolayer for plasmonic Color Modulation. *ACS Appl. Nano Mater.* **2021**, *4* (9), 9721−9728.

https://doi.org/10.1021/acsomega.3c05707
ACS Omega 2023, 8, 41579−41585

(45) Sun, Y.; Xia, Y. Shape-Controlled Synthesis of Gold and Silver Nanoparticles. *Science* **2002**, *298* (5601), 2176−2179.
(46) Im, S. H.; Lee, Y. T.; Wiley, B.; Xia, Y. Large-Scale Synthesis of Silver nanocubes: The Role of HCl in Promoting Cube Perfection and Monodispersity. *Angew. Chem., Int. Ed.* **2005**, *44* (14), 2154−2157.
(47) Chang, S.; Chen, K.; Hua, Q.; Ma, Y.; Huang, W. Evidence for the Growth Mechanisms of Silver nanocubes and nanowires. *J. Phys. Chem. C* **2011**, *115* (16), 7979−7986.
(48) Chen, Z.; Balankura, T.; Fichthorn, K. A.; Rioux, R. M. Revisiting the Polyol Synthesis of Silver nanostructures: Role of Chloride in nanocube Formation. *ACS Nano* **2019**, *13* (2), 1849−1860.

https://doi.org/10.1021/acsomega.3c05707
ACS Omega 2023, 8, 41579−41585